DOI: https://doi.org/10.14311/TPFM.2025.024

NUMERICAL INVESTIGATION OF BI-DIMENSIONAL FLOW IN A ROTATING SPHERICAL LID-DRIVEN CYLINDRICAL CAVITY

A. Meziane, F. Yahi, A. Benbrik

Department of Transport and Hydrocarbon Equipment, Faculty of Hydrocarbons and Chemistry M'Hamed Bougara Boumerdes University, Independence Avenue, 35000 Boumerdes, Algeria.

Abstract

Our work focuses on a numerical study of axisymmetric flows, of a viscous and incompressible fluid, generated by rotating the spherical end disks of a cylindrical or truncated conical cavity. The numerical simulation has revealed various secondary flow structures, due to the combined effects of the rotating and/or stationary boundaries, whose nature and number depend on the physical parameters $\mathrm{Re} = \Omega_b R^2_{0b}/\nu$ (the Reynolds number) and on the radius ratio of the enclosure $\Lambda = R_2/R_1$. In the case of a cylindrical cavity whose aspect ratio $\Lambda \geq 1.48$, the study reveals the occurrence of axisymmetric bubbles, in the vicinity of the rotating axes, characterised by a stagnation point and an inverse flow (vortex breakdown).

Keywords: rotating disks, co and contra-rotation, vortex breakdown, boundary effects

1 Introduction

In cylindrical rotor-stator cavities, with radius ratio $\Lambda > 1$, even moderate rotate rates can lead to stagnation points. The latter are located on the axis of the cavity, followed by zones of reverse flow in the vicinity of this axis [1], [2]. These recirculation zones, of low intensity compared to the base flow, appear in the meridian plane in the shape of a bubble, with limited radial and azimuthal extension; commonly characterize the phenomenon of vortex breakdown in a confined middle [3]. In this study, we are exclusively interested in axisymmetric structures in steady state. It should also be noted that, unlike certain vortex structures (for example boundary layer instability) [4], [5], which appear, for very high rotations, in the vicinity of the walls, vortex breakdown develops for moderate Re in the central core of the flow, considered practically not very viscous, in quasi-solid rotation [6]. In the literature that we have reviewed [7], this physical phenomenon in the case of closed cavities of the cylindrical "rotor-stator" type was studied, experimentally, for the first time by Vogel [8]. A series of systematic experiments, carried out in this configuration, allowed Escudier [7] to constitute, for the first time, a diagram in the plane (Λ, Re) indicating the flow regimes with or without vortex region, as well as the boundary curves delimiting the stationary and unsteady regimes. In this work, the operating domain is placed within the framework of the new diagram.

2 Geometric and mathematical modelling of confined flow

Consider the flow in a truncated conical cavity, driven by spherical covers, of radii R_1 and R_2, which rotate with constant, but different, angular velocities Ω_b and Ω_t, respectively (Fig.1a). Numerical results undertaken in the confined cavities will be presented in several geometrical configurations. We note that for example if $R_{0t} = R_1 \sin\theta$, $R_{0b} = R_2 \sin\theta$ corresponds to the truncated enclosure; if $R_{0t} = R_{0b} = R_1 \sin\theta$ corresponds to the cylindrical cavity (Fig.1b).

Table 1: Geometric and dynamic control parameters:

Reynolds number	Radius fraction	Characteristic length of discs
$R_e = \dfrac{\Omega_b R^2}{\nu}, R = R_2 \sin\vartheta$	$\Lambda = R_2/R_1$	R_{0b}, R_{0b}.

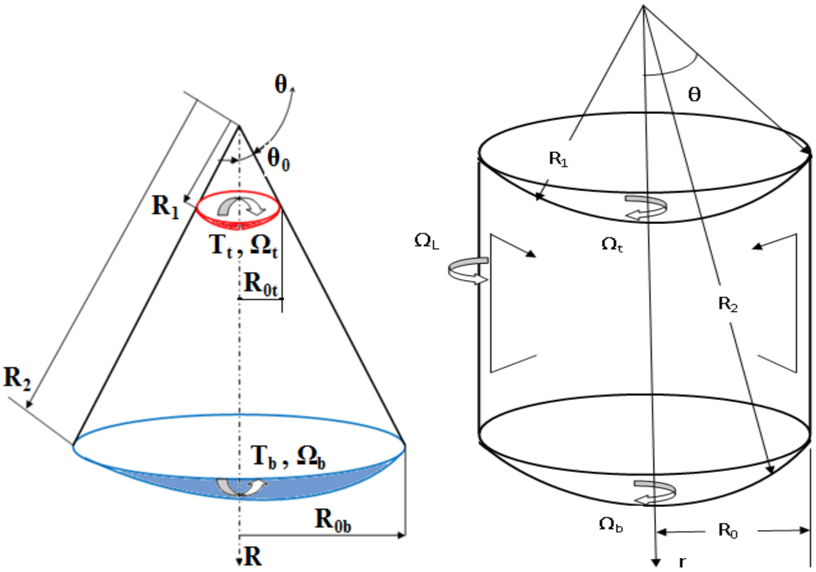

Figure 1: schematic of the problem in truncated conical cavity with spherical end disks.

The components of the velocity in directions r, θ and Φ are u, v and w, respectively. These velocity components for incompressible flow and in a meridian plane satisfy the continuity equation, being related to a stream function $\Psi(r,\theta)$ and a swirl function $\Omega(r,\theta)$, in the following manner:

$$u(r,\theta)=\frac{1}{r^2\sin\theta}\frac{\partial\psi}{\partial\theta},\ v(r,\theta)=-\frac{1}{r\sin\theta}\frac{\partial\psi}{\partial r},\ w(r,\theta)=\frac{\Omega}{r\sin\theta}$$

Since, the flow is assumed to be independent of the longitude Φ, the governing equation of the flow can be written as:

$$\frac{\partial\Omega}{\partial t}r^2\sin\theta+\frac{\partial(\psi,\Omega)}{\partial(r,\theta)}=\frac{r^2\sin\theta}{Re^2} \tag{1}$$

$$\frac{\partial\zeta}{\partial t}\cdot r^2\sin\theta+2\Omega\left(\cot\theta\frac{\partial\Omega}{dr}-\frac{1}{r}\frac{\partial\Omega}{\partial\theta}\right)+2\zeta\left(\cot\theta\frac{\partial\psi}{\partial r}-\frac{1}{r}\frac{\partial\psi}{\partial\theta}\right)-\frac{\partial(\psi,\zeta)}{\partial(r,\theta)}=\frac{r^2\sin\theta}{Re^2} \tag{2}$$

Where:

$$D^2=\frac{\partial^2}{\partial r^2}+\frac{1}{r^2}\frac{\partial^2}{\partial\theta^2}-\frac{\cot\theta}{r}\frac{\partial^2}{\partial\theta^2}$$

and

$$\frac{\partial(\psi,\Omega)}{\partial(r,\theta)}=\frac{\partial\psi}{\partial r}\frac{\partial\Omega}{\partial\theta}-\frac{\partial\psi}{\partial\theta}\frac{\partial\Omega}{\partial r}$$

The boundary conditions for the above governing equations are:
The no-slip boundary conditions on the lids $0\le\theta\le 20^{o}$:

$$\begin{cases} R=R_1:\Omega(R_1,\theta)=\Omega_t\sin^2\theta,\psi(R_1,\theta)=\dfrac{\partial\psi}{\partial R}(R_1,\theta)=0 \\ R=R_2:\Omega(R_2,\theta)=\Omega_b\sin^2\theta,\psi(R_2,\theta)=\dfrac{\partial\psi}{\partial R}(R_2,\theta)=0 \end{cases} \tag{3a}$$

The symmetry condition on the axis $\theta_0 = 0$:

$$\psi=0, D^2\psi=0, \Omega=0 \tag{3b}$$

At the sidewall $\theta_0 = 20°$:

$$\Omega(R,\theta_0)=\Omega_L R^2\sin^2\theta_0,\psi(R,\theta_0)=0,\frac{\partial\Psi}{\partial\theta}(R,\theta_0)=0 \tag{3c}$$

3 Results and discussion

3.1 Numerical method

To solve the above system, a finite volume method is used to solve Eqs. (1) and (2). This well-established code has been used extensively in the calculation of complex flows and, with the correct implementation, is adequate to model the laminar flows under consideration here. We used the segregated solver in which the momentum and swirl velocity equations were discretised using a second-order upwinding scheme. Coupling of the pressure and velocity was achieved using the well-known SIMPLEC implementation. Double precision (2ddp) was used for all the calculations so that round-off errors are negligible. In general the scaled residuals were observed to reach a level between $1 \times 10^{-7}$and 1×10^{-9}. Firstly we made a qualitative comparison between our calculated streamlines and the experimental visualisations of K.Bühler [9]. Such a comparison is shown good agreement in Fig. 2.A grid independency test has been conducted for the case of a α = 2.0 cylindrical cavity with rotating spherical bottom lid at Re = 2000. A preliminary series of calculations was carried out with A(30 /60), B(40 /80), D(110/150) and E(150×200) uniform cells to investigate the accuracy of our simulations . As can be seen the simulation predicts both the occurrence of the primary and secondary recirculation bubbles as well as their size and location along the centreline, Fig. 3. The mesh sizes above are (r×θ) in directions. In addition to this qualitative comparison, a series of quantitative estimation of maximal contour of Ψ (table 1) show that the error between D (110×150) and E (150× 200) is about 0.8% at most and so can be regarded as negligibly small. The fine grid resolution was selected for all simulations.

(a) **(b)**

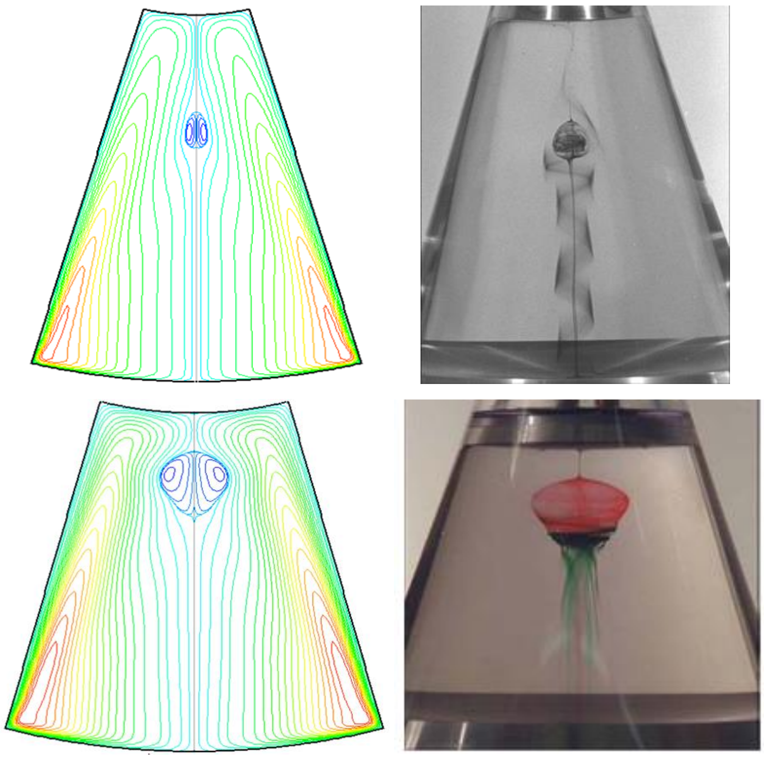

Figure 2: Comparison of computed streamlines (a) and experimental flow visualisation (b) (taken from K.Bühler [9] of flow produced in a truncated conical container; $\Lambda = 3.06$; $\alpha = 2$; $\theta_0 = 15^0$; Re = 5000,3600.

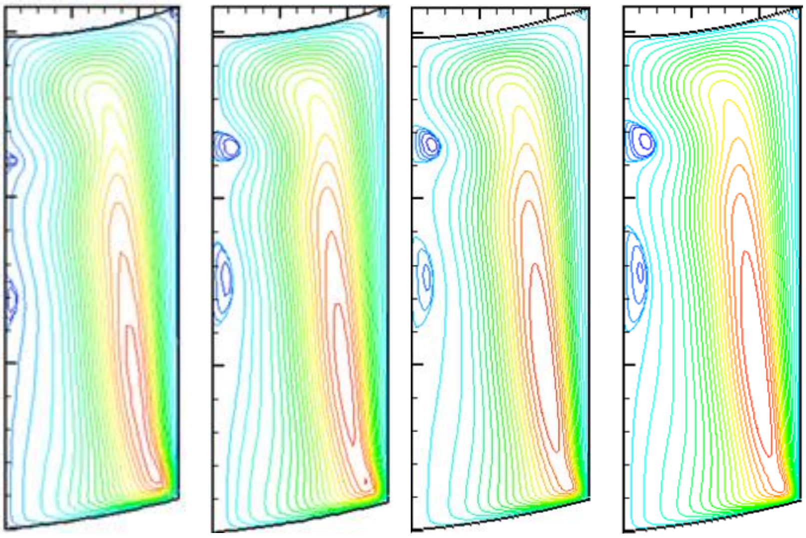

Figure 3: Comparison of stream function with vortex breakdown, of four test cases A (30 /60), B (40 /80), D (110/150) and E (150×200); $\Lambda = 2$; $\mathrm{Re} = 644, \theta = 20^0$.

Table 2: Mesh characteristics for the case $\Lambda = 2$; $\mathrm{Re} = 644$

$(r\times\theta)$	A(30×60)	B(40×80)	C(60×100)	D(110×150)	E(150×200)
Ψ_{max} (10^{-5}) kg/s	1.67768	1.663139	1.653687	1.618053	1.59475
Nodes used	1892	3201	6162	16762	30351

3.2 Isothermal flow in a cylindrical cavity with a rigid surface

3.2.1. Solution domain

The stationary base flow generated in the cylindrical rotor-stator cavity (S = 0) by the rotation of the lower disk is presented in the range of control parameters: $1.68 \leq \Lambda \leq 3.06$; $350 \leq \mathrm{Re} \leq 1300$, $0 \leq \theta \leq 20^\circ$.

3.2.2. Description of the basic flow S=0 (where S is the disk rotation rate ratio):

The global structure of the steady flow resulting from the rotation of the lower disk from a cylindrical configuration with spherical covers of radius ratio Λ=3.06 is analyzed, for Re=1000; 1300. From a qualitative point of view, for the rotation rates and the radius ratio considered, the global flow consists of three distinct boundary layers where the viscosity effects developed in the vicinity of the solid walls of the cavity are concentrated. In connection with these boundary layers, a relatively low-viscosity, rotating central nucleus can be distinguished. These flows are generally classified as Batchelor flows [10]. By extension of the definitions relating to boundary layers, developed on disks of infinite meridional extension, the boundary layer formed on the rotating disk (rotor) is assimilated to an Ekman boundary layer, and that developed on the fixed disk to a Bödewadt layer. These different zones result from the combined influence of each of the walls of the closed cavity, giving rise to a secondary flow, in the meridian plane, which is superimposed on the basic rotation initiated by the rotating disk, figure (4-a). The global view of this secondary flow is given by the plot of the iso-values of the stream function, figure (4-a), of the tangential vorticity, figure (4-c) as well as by the iso-circulations, figure (4-b). Indeed, under the effect of viscous constraints, the fluid undergoes a centrifugal meridional circulation on the rotating disk, where a boundary layer called Ekman is formed; figure (4-c), the thickness of which, for these indicated parameters, remains almost constant outside the turning zone of the outer envelope. The presence of the fixed lateral confinement imposes an upward axial circulation on the fluid, over a thickness $\delta(R_{0b})$ which extends along the fixed envelope (recirculation boundary layer), figure (4-c). By continuity, the fluid in the core of the flow is sucked towards the rotating disk (rotor), by Ekman pumping effect, while a centripetal meridional circulation develops on the fixed disk attached to the outer envelope; with formation of a Bödwadt type boundary layer, figure (4-c). We note the axial dependence of the recirculation layer (cylindrical wall), which thickens as the flow approaches the fixed disk, and connects to the Bödwadt boundary layer formed on the latter. It should be noted that no substantial meridional dependence of the Bödwadt layer was observed in the pairs of parameters Λ and Re used. The influence of the Reynolds number is illustrated in this same figure (Figure 4), which indicates a slight thinning of the thickness of the high gradient zones when Re increases. The iso-lines of the circulation (figures (4-b_1-b_2)) reveal that, the angular momentum (Γ), is practically independent of R_{0b} in the central core of the flow; indicating a quasi-solid rotation of the fluid. Furthermore, angular momentum Γ reaches a maximum in the vicinity of the peripheral of the rotating disk. The velocity field, characterizing the meridional flow, is illustrated by the axial distribution of (u) and the radial distribution of (w) for Re = 1000 and $\Lambda = 3.06$, figures (6_a, 6_b). A simultaneous analysis of figures (6_a, 6_b) highlights this meridional flow and its direction, and confirms the areas with high gradients. Furthermore, we observe in Figure 5 that the radial profile of the circulation Γ, showing a parabolic shape practically independent of R_{0b}, in the vicinity of the core ($0 \leq R_{0b} \leq 0.02$), indicates that the angular momentum (in this zone) transports the fluid practically in quasi-solid rotation with a relatively low angular velocity. Near the walls, the variations are very pronounced depending on the distance (R_{0b}).

Re=1000 (a_1) (b_1) (c_1)

Re=1300 (a_2) (b_2) (c_2)

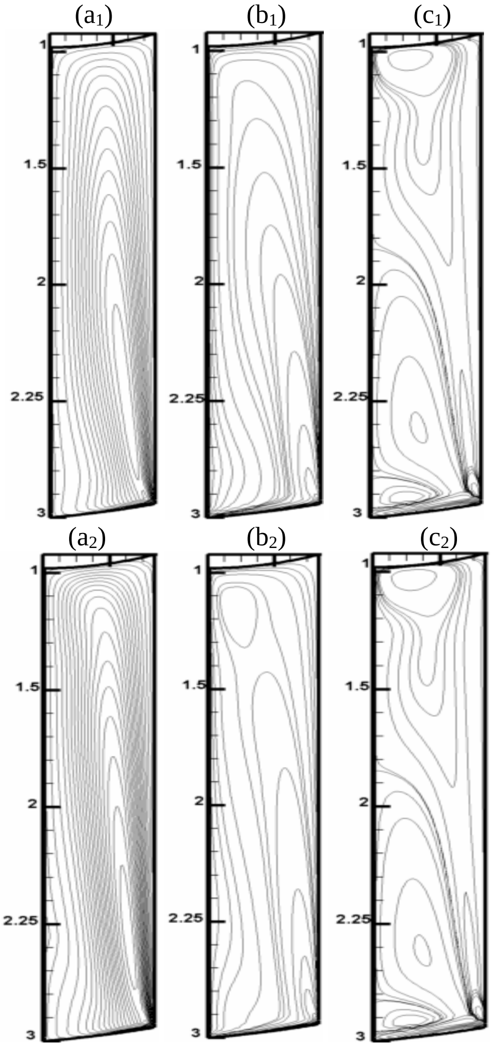

Figure 4: (a_1, a_2) Streamlines, (b_1, b_2) Iso-circulation,(c_1, c_2) Iso-vorticity; $\Lambda = 3.06; \theta = 20^0, S = 0$, Re as indicated.

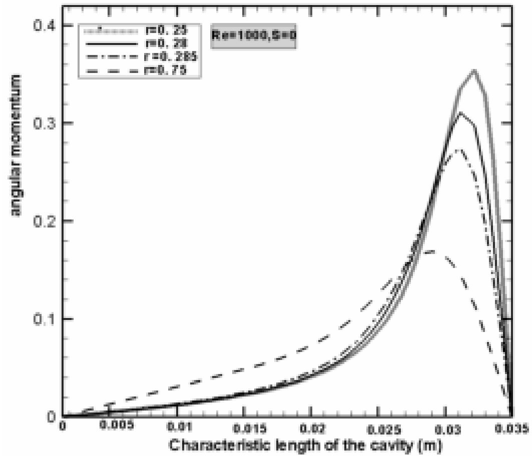

Figure 5: Radial evolution of circulation Γ, Λ = 3.06.

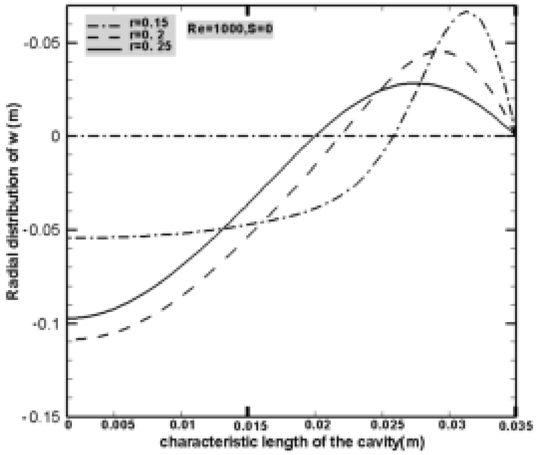

Figure 6a: Radial distribution of *W* Λ=*3.06.*

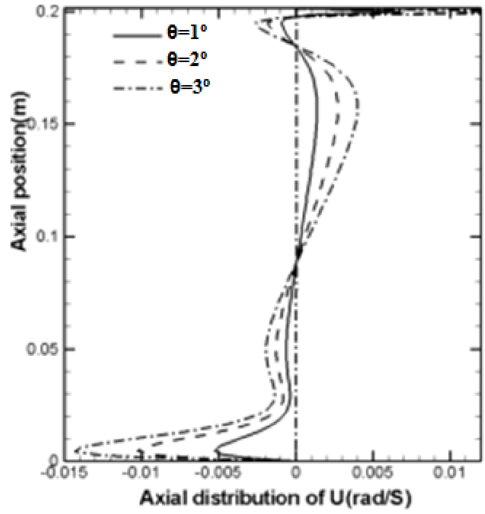

Figure 6b: Axial distribution of *u;* Λ=*3.06.*

3.2.3. Global description of the vortex breakdown: highlighting a recirculation zone

In this part, we highlight the recirculation zones which are superimposed on the basic flow, generated by the rotation of the lower disk of a rotor-stator type cavity (S = 0). By progressively varying the Reynolds number Re, for a fixed radius ratio Λ = 1.68, the development of a reverse recirculation zone was highlighted; preceded upstream by a stagnation point. The critical number Re_c of appearance, corresponding to this configuration, is $Re_{c1} = 373$. Figure 7, showing the azimuthal stream, circulation and vorticity lines; clearly illustrate the steps of formation and evolution of the bubble, located in the vicinity of the cavity axis. For disk rotation rates such as $Re_{c1} < Re$, the basic flow indicates a central (axial), low-viscosity, relatively quasi-solid rotation, figure (7-b_1). This is characterized by a balance between the radial pressure gradient and the centrifugal acceleration. In the vicinity of the critical Reynolds $Re_{c1} \approx 373$, a centrifugal imbalance occurs in this core which contributes to slowing down and cancelling the meridional component of the velocity on the axis, followed by a deflection (divergence) of the streamlines, figure (7-a_2, a_3). Furthermore, by continuing to increase Re, the stationary solutions reveal a decrease in the size of the bubble until its disappearance when $Re_{c2} = Re = 820$, figure (7-a_4). In the disappearance process, figure 7 indicates a slight radial displacement of the bubble towards the fixed disk. It should be noted that the critical thresholds of appearance, Re_{c1}, and disappearance Re_{c2}, of the vortex breakdown, in rotor-stator configuration for Λ = 1.68, S = 0, are in very good agreement with the boundary curves of Escudier [7].

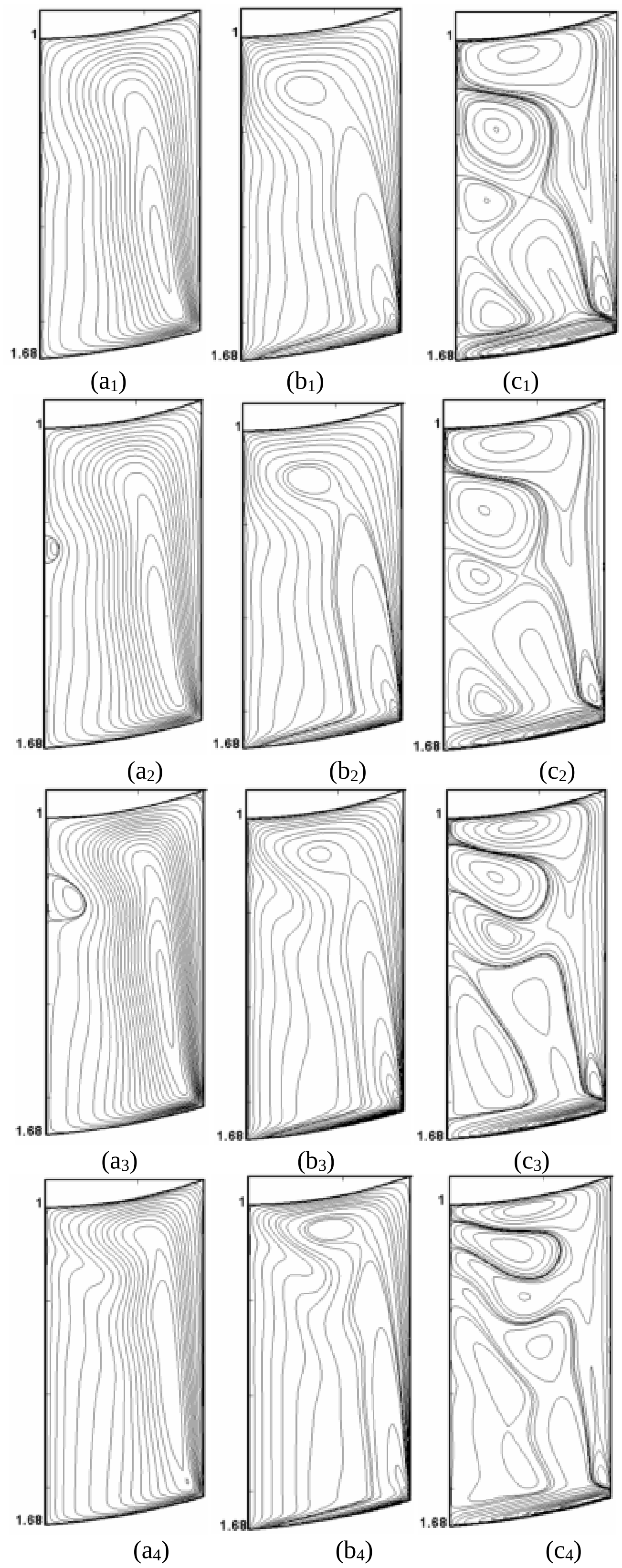

Figure 7: (a_1 - a_4) streamlines, (b_1 - b_4) iso-circulation, (c_1 - c_4) iso-vorticity; $S = 0, \Lambda = 1.68$, $\theta_0 = 20°$; (a) Re = 350, (2) Re = 373, (3) Re = 522, (4) Re = 820.

Conclusion

This work allowed us to highlight and analyze qualitatively and quantitatively a secondary flow zone, in the meridian plane, resulting from the influence of rotating and/or fixed walls. The number of these cells, their location, their direction of rotation and their evolution are dictated by the choice of the parameters Re and Λ : $350 \leq Re \leq 1300$ et $1.68 \leq \Lambda \leq 3.06$. The simulation of the flow in a cylindrical cavity of the rotor-stator type (S = 0), with aspect factor $\Lambda > 1$, revealed a structure composed of a boundary layer on each solid wall; centrifugal on the rotating disk (Ekmán or von Kármán), centripetal on the fixed disk (Bödwadt) and by a weakly rotating central core.

References

[1] Serre, E. & Bontoux, P. : Eclatement tourbillonnaire dans une cavité rotor–stator cylindrique. *Comptes Rendus de l'Académie des Sciences-Series IIB- Mechanics*, 329(9), (2001), pp. 671-677

[2] Meziane, A., Hachemi, M., Kessal, M., & Imoula, M.: A Wall Effects and Means of Controlling the Evolution of Swirling Flows with Vortex Breakdown. *Journal of Applied Fluid Mechanics*, 16(11), (2003), pp. 2277-2289

[3] Lopez, J. M.: Axisymmetric vortex breakdown flow. *Journal of Fluid Mechanics*, 221, (1990), pp. 533- 552.

[4] Yahi F., Hamnoune Y., Bouabdallah A., Lecheheb S., Mokhtari F.: Experimental Investigation of the Free Surface Effect on the Conical Taylor-Couette Flow System. *Journal of Applied Fluid Mechanics*, Vol. 9, No. 6, (2016), pp. 2743-2751.

[5] Yahi F., Hamnoune Y., Hellalbi M. A., Tigrine Z., Merabet N., Meziane A., Bouabdallah A.: Numerical Approach of the Differential Heating Effect on a Fluid Enclosed between Two Coaxial Cones, In *Proceedings Topical Problems of Fluid Mechanics 2024*, Prague, 2024, Edited by David Šimurda and Tomáš Bodnár, pp. 263, ISSN 2336-5781 ,
DOI: https://doi.org/10.14311/TPFM.2024.035.

[6] Sorensen, J.N., Christensen, E.A.: Direct numerical simulation of rotating fluid flow in a closed cylinder, *Phys. Fluids.*7, 764 (1995).

[7] Escudier, M. P.: Observations of the Flow Produced in a Cylindrical Container by a Rotating End Wall, *Experiments in Fluids*, 2(4), (1984), pp. 189-196.

[8] Vogel, H. U,: Experimetelle Ergebnisseueber die Laminare Stroemung in einemzylindrischen Gehaeusemitdarinrotierender Scheibe. Max Planck Institut fur Stromungs Forschung, Gottingen Bericht, 6 (1968).

[9] Bühler, K.: Pattern formation in rotating fluids. *Journal of Thermal Science*, 18(2), 109, (2009).

[10] Batchelor G.K.: An Introduction to Fluid Dynamics, Cambridge University Press, Cambridge (1967).